Korean J. Chem. Eng., 40(7), 1616-1622 (2023)
DOI: 10.1007/s11814-023-1426-y

pISSN: 0256-1115
eISSN: 1975-7220

Model-based fault detecting strategy of urea-selective catalytic reduction (SCR) for diesel vehicles

Sanha Lim and Jong Min Lee†

School of Chemical and Biological Engineering, Institute of Chemical Processes, Seoul National University, Gwanak-ro 1, Gwanak-gu, Seoul 08826, Korea
(*Received 12 October 2022 • Revised 6 January 2023 • Accepted 31 January 2023*)

Abstract−Selective catalytic reduction (SCR) is diesel aftertreatment using a reduction agent to reduce nitrogen oxides. Diesel engine regulations are being tightened; therefore, the diesel aftertreatment system should be operated efficiently. In the urea-SCR system, there is a possibility of various faults, e.g., catalyst deactivation by sulfur or hydrothermal aging and fault in urea injection system. These faults interfere with normal system operation and result in increase of NOx concentration at the tailpipe. To prevent this situation, it is necessary to detect system faults. In this study, a first-principle model for SCR system is presented based on mass and energy balance equations. Using the one-dimensional urea-SCR model, this research introduces a model-based fault detecting strategy for SCR system. The residuals are calculated as the difference between the model calculation and the actual catalyst system measurement with the system faults. The results of this research are used in fault diagnosis and fault tolerant control studies to meet diesel vehicle nitrogen oxide regulations even in the presence of catalyst faults.

Keywords: Selective Catalytic Reduction, Model-based, Fault Detection, Aftertreatment System, Diesel Vehicle

INTRODUCTION

Diesel engines have better fuel efficiency and longer life cycle than gasoline engines [1,2]. For this reason, they are used in transportation, construction, and many industrial applications. However, despite many advantages, air pollutants from diesel engine, such as carbon monoxide (CO), hydrocarbons (HC), particulate matter (PM) and nitrogen oxides (NOx), contribute to environmental problems [3]. With global environmental issues emerging, regulations on emissions from diesel automobile have been tightened. Accordingly, an aftertreatment system has become essential for diesel vehicles. Carbon monoxide, unburned hydrocarbons are removed using diesel oxidation catalyst (DOC) [4]. Diesel particulate filter (DPF) filters particulate matter (PM) from diesel engine and burns it at high temperatures [5,6]. Nitrogen oxides can be reduced through an engine gas recirculation (EGR) system, but with the introduction of Euro 6 regulations in 2014, additional aftertreatment systems such as lean NOx trap (LNT) and selective catalytic reduction (SCR) began to be inevitable. From September 2017, the Euro 6c regulation, which applied real-driving emission (RDE) test, was implemented, making the regulation of nitrogen oxide emissions more stringent [7,8]. As a result, the future of eco-friendly diesel vehicles faces the challenge of deNOx in real driving conditions.

Various studies have been conducted to efficiently reduce nitrogen oxides from diesel vehicles [9-12]. Among them, the urea-SCR system has a high NOx conversion rate at high temperatures [13,14], and does not require additional fuel consumption which is essential for LNT system [15]. The aftertreatment system equipped with urea-SCR is shown in Fig. 1. CO, HC and PM from diesel engines are removed in DOC and DPF. Urea solution is injected from the urea injector to remove nitrogen oxides in the SCR module. The injected urea is decomposed by the high temperature of exhaust gas [16]. One molecule of urea produces two molecules of ammonia as follows:

$$(NH_2)_2CO \rightarrow NH_3 + HNCO \quad (1)$$

$$HNCO + H_2O \rightarrow NH_3 + CO_2 \quad (2)$$

The generated ammonia is adsorbed onto the adsorption sites S1 and S2 [17]. The ammonia adsorbed on S1 site does not chemically react with nitrogen oxides. At each site, desorption of ammonia also occurs.

$$S1 + NH_3 \rightarrow NH_3 - S1 \quad (3)$$

$$NH_3 - S1 \rightarrow S1 + NH_3 \quad (4)$$

$$S2 + NH_3 \rightarrow NH_3 - S2 \quad (5)$$

$$NH_3 - S2 \rightarrow S2 + NH_3 \quad (6)$$

Desorbed ammonia molecules in gas phase are consumed by oxygen at high temperature. The oxidation reactions generate nitric oxide and nitrous oxide. Nitric oxide also reacts with oxygen at high temperature to be equilibrated with nitrogen dioxide.

$$NH_3 + \frac{5}{4}O_2 \rightarrow NO + \frac{3}{2}H_2O \quad (7)$$

$$NH_3 + \frac{3}{4}O_2 \rightarrow \frac{1}{2}N_2 + \frac{3}{2}H_2O \quad (8)$$

$$NH_3 + O_2 \rightarrow \frac{1}{2}N_2O + \frac{3}{2}H_2O \quad (9)$$

†To whom correspondence should be addressed.
E-mail: jongmin@snu.ac.kr

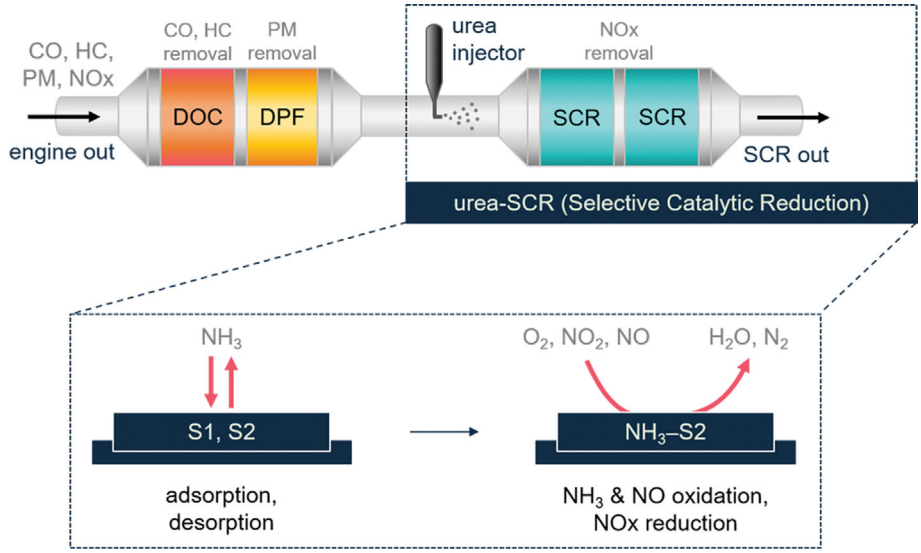

Fig. 1. Scheme of diesel aftertreatment system with urea-SCR.

$$NO+\frac{1}{2}O_2\rightarrow NO_2 \tag{10}$$

Ammonia stored in the S2 site is used as a reducing agent in the SCR reactions to eliminate NOx. There are three types of SCR reactions: standard SCR, fast SCR and NO_2 SCR. In the standard SCR reaction, ammonia and nitric oxide react in 1 : 1 stoichiometric ratio, to generate nitrogen and water. The fast SCR reaction consumes both nitric oxide and nitrogen dioxide [18]. The NO_2 SCR reaction employs nitrogen dioxide only [19].

$$NH_3-S2+NO+\frac{1}{4}O_2\rightarrow S2+N_2+\frac{3}{2}H_2O \tag{11}$$

$$NH_3-S2+\frac{1}{2}NO+\frac{1}{2}NO_2\rightarrow S2+N_2+\frac{3}{2}H_2O \tag{12}$$

$$NH_3-S2+\frac{3}{4}NO_2\rightarrow S2+\frac{7}{8}N_2+\frac{3}{2}H_2O \tag{13}$$

$$NH_3-S2+\frac{5}{4}NO_2\rightarrow S2+\frac{1}{8}N_2+N_2O+\frac{3}{2}H_2O \tag{14}$$

Through the above reactions, NOx from diesel vehicles is converted into harmless nitrogen and water. Urea-SCR system is able to reduce more than 90% of NOx from the exhaust gas. However, when a fault occurs in the urea-SCR system, the NOx reduction efficiency decreases and the amount of emission increases. Recently, automobile manufacturers have been building fault detecting systems in order to meet on-board diagnostics (OBD) regulations, which monitor the conditions of the vehicle. It is necessary to systematically determine whether the aftertreatment system operates normally while driving, because the requirements of OBD regulations are increasing as the Euro regulations are stringent [20]. Possible fault scenarios of urea-SCR include problems with the urea injection system and catalyst aging.

Failure of a dosing pump or a clogged urea injector nozzle hinders proper urea injection. If an insufficient amount of urea solution is injected, the SCR system will not function properly [21]. In addition, the performance of the SCR system is also susceptible to catalyst aging. Sulfur in the exhaust gas of diesel engines often blocks the active site of the SCR catalysts [22]. Furthermore, SCR catalysts are vulnerable to hydrothermal aging due to high temperature and water [23]. The deactivated catalyst significantly lowers the NOx conversion, causing a large amount of NOx to be emitted into from the tailpipe.

Therefore, it is crucial to detect and diagnose SCR system faults to prevent system failure. This paper suggests a fault detecting strategy for urea-SCR system. Fault scenarios are identified by generated residuals using a mathematical model with high-fidelity. This paper is organized as follows: Section 2 presents the mathematical modeling approach for urea-SCR system and model-based fault detection strategy. The results of model-based fault detection with two fault scenarios are shown in Section 3. Finally, Section 4 provides the concluding remarks.

METHODOLOGIES

1. Urea-SCR Model

In this research, a fault detecting strategy is presented using a one-dimensional model of urea-SCR. The governing equations for the first-principle model are derived based on the differential volume [15,24]. The mass balance equation for the species j in the bulk gas phase is

$$\frac{\partial(C_{g,j}V_g)}{\partial t}+\frac{\partial(u_gC_{g,j}V_g)}{\partial z}+k_{m,j}A_{wc-g}(C_{g,j}-C_{wc,j})=0 \tag{15}$$

which can be rewritten as

$$\frac{\partial C_{g,j}}{\partial t}+u_g\frac{\partial C_{g,j}}{\partial z}=-\frac{k_{m,j}A_{wc-g}}{V_g}(C_{g,j}-C_{wc,j}) \tag{16}$$

where $C_{g,j}$ and $C_{wc,j}$ are the mole concentration of species j in the bulk gas phase and washcoat phase, respectively. Other notations of the governing equations are in the nomenclature section. The species j in the bulk gas phase diffuses into the washcoat phase with

convective mass transfer coefficient $k_{m,j}$, which is calculated using collision theory [25]. Collision theory considers collision diameter $\sigma_{j,air}$ and collision integral $\Omega_{j,air}$ of the species j. The shape of all channels was assumed to be a square in order to set the proper Sherwood number [26].

$$k_{m,j}=\frac{Sh\cdot D_{mol,j}}{d_h} \tag{17}$$

$$D_{mol,j}=5.95432\cdot 10^{-24}\frac{\sqrt{T^3\left(\frac{1}{M_{air}}+\frac{1}{M_j}\right)}}{p_0\sigma_{j,air}^2\Omega_{j,air}} \tag{18}$$

The convective mass transfer coefficient $k_{m,j}$ is proportional to molecular diffusivity coefficient $D_{mol,j}$, which is affected by temperature and collision integral. The collision integral $\Omega_{j,air}$ can be calibrated based on the collision integral table [27]. The thermal energy of bulk gas is transferred to the washcoat on the catalyst surface. The energy balance equation in the bulk gas phase is written as

$$\frac{\partial(T_g\rho_g c_{p,g}V_g)}{\partial t}+\frac{\partial(u_g T_g\rho_g c_{p,g}V_g)}{\partial z}+U_o A_{wc-g}(T_g-T_{wc})=0 \tag{19}$$

or

$$\frac{\partial T_g}{\partial t}+u_g\frac{\partial T_g}{\partial z}=-\frac{U_o A_{wc-g}}{\rho_g c_{p,g}V_g}(T_g-T_{wc}) \tag{20}$$

where U_o is the overall heat transfer coefficient and u_g is bulk gas velocity. It is assumed that all channels have the same flow rate.

In the washcoat phase, chemical species diffuse in and out from the bulk gas phase. Each chemical component participates in the reactions to be consumed or generated. In this process, the heat of reaction is released or absorbed. The mass balance equation of washcoat phase is written as

$$\frac{\partial(C_{wc,j}\varepsilon_{wc}V_{wc})}{\partial t}+\frac{\partial(u_{wc}C_{wc,j}\varepsilon_{wc}V_{wc})}{\partial z}+k_{m,j}A_{wc-g}(C_{wc,j}-C_{g,j}) \tag{21}$$
$$+\sum_i \nu_{ji}r_i V_{cat}=0$$

The gas velocity on the washcoat surface u_{wc} is negligible since no-slip condition is assumed. Eq. (21) can be rewritten as

$$\varepsilon_{wc}\frac{\partial C_{wc,j}}{\partial t}=k_{m,j}G_a(C_{g,j}-C_{wc,j})-\sum_i \nu_{ji}r_i \tag{22}$$

where ε_{wc} is washcoat porosity and $G_a=A_{wc-g}/V_{cat}$. For energy balance equations, reaction heat is considered. Since the washcoat phase is in contact with the substrate phase, heat transfer between the two phases must be also considered.

$$\frac{\partial(T_{wc}\rho_{wc}c_{p,wc}V_{wc})}{\partial t}+\sum_{i,j}\nu_{ji}r_i H_j^f V_{cat}+U_o A_{wc-g}(T_{wc}-T_g) \tag{23}$$
$$+U_{o,s}A_{wc-s}(T_{wc}-T_s)=0$$

For substrate phase, heat transfer via conduction and radiation is ignored. The catalytic module is assumed adiabatic.

$$\frac{\partial(T_s\rho_s c_{p,s}V_s)}{\partial t}+U_{o,s}A_{wc-s}(T_s-T_{wc})=0 \tag{24}$$

Combining Eqs. (23) and (24), the following equation can be obtained:

$$\frac{\partial(T_{wc}\rho_{wc}c_{p,wc}V_{wc})}{\partial t}+\sum_{i,j}\nu_{ji}r_i H_j^f V_{cat}+U_o A_{wc-g}(T_{wc}-T_g) \tag{25}$$
$$+\frac{\partial(T_s\rho_s c_{p,s}V_s)}{\partial t}=0$$

Assuming $T_s=T_{wc}$, the energy balance equation of washcoat phase can be written as

$$(\varepsilon_2\rho_{wc}c_{p,wc}+\varepsilon_3\rho_s c_{p,s})\frac{\partial T_{wc}}{\partial t}=U_o G_a(T_g-T_{wc})-\sum_{i,j}\nu_{ji}r_i H_j^f \tag{26}$$

where $\varepsilon_2=V_{wc}/V_{cat}$ and $\varepsilon_3=V_s/V_{cat}$. The kinetic parameters to calculating each reaction rate r_i, are adopted from the authors' previous work [28]. The coverage fraction of adsorption sites is considered as

$$\frac{\partial\theta_m}{\partial t}=\frac{\Sigma_i\nu_{mi}r_i}{\psi_m} \tag{27}$$

where θ_m is coverage fraction of each site and ψ_m is storage capacity.

Since partial differential equations are included in the governing equations, they need to be in a simpler form to be calculated in the engine control unit (ECU). The equations are simplified using the successive linearization method [29]. As shown in Fig. 2, the single-channel model is discretized in the z-direction. Within a sufficiently small compartment L_z, the derivative of state in z direction can be assumed to be linear form as

$$\frac{\partial C_{g,j}}{\partial z}\cong\frac{C_{g,j}^{(n)}-C_{g,j}^{(n-1)}}{L_z} \tag{28}$$

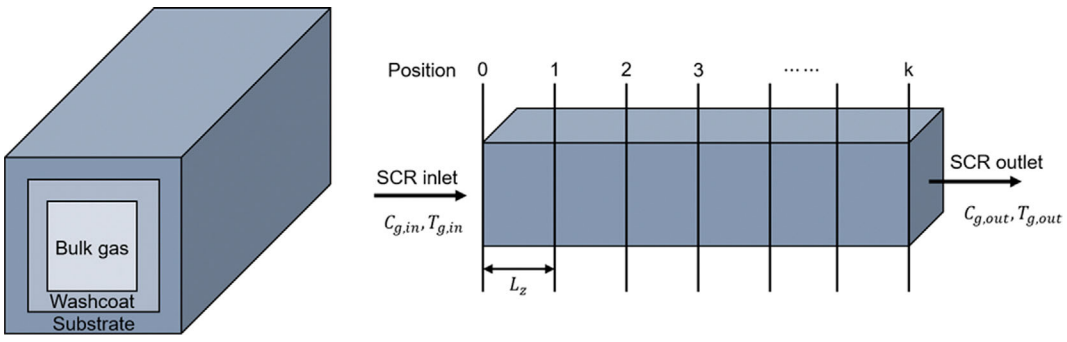

Fig. 2. Discretization of a single channel in z direction.

$$\frac{\partial T_g}{\partial z} \cong \frac{T_g^{(n)} - T_g^{(n-1)}}{L_z} \quad (29)$$

for n=1, 2, ⋯, k, where $C_{g,j}^{(n)}$ and $T_g^{(n)}$ represent the mole concentration and temperature in *n*th position. Through this method, the number of states and equations is increased k times, but the PDE can be converted into multiple ODEs. The smaller L_z is, the more accurate simulation is possible. Although a two-cell model was proposed in a previous paper [30], k is set to 5 in this study to minimize model-plant mismatch.

2. Model-based Fault Detection

Recently, data-based fault detection studies have been conducted in the field of chemical engineering [31,32]. However, data-based fault detection methodologies are usually suitable for large scale processes, which have numerous sensors of operating units. On the contrary, aftertreatment system of diesel vehicles has limited measurable variables. It is also inaccessible to obtain the driving data with system faults. The model-based fault detection approach has been widely adopted in various industries [33,34]. Based on measured input and output, the model-based methods use dynamic process model. These methods are based on parity equations, parameter estimation and state observers [35]. Among them, the parity equation approach uses a process model to generate an output error, comparing the behavior of the actual process [36]. If the dynamic model matches the actual process and the sensors are fault free, the model can be used to identify presence of fault in the system. As shown in Fig. 3, the residuals are generated by comparing the two model, SCR system without any fault and SCR system with system fault. It is assumed that three measurements are possible at outlet stream: NOx concentration, NH_3 concentration and temperature. As shown in Eqs. (30), (31) and (32), three residuals are calculated by simply comparing the three real-time measurements. This simple calculation is also possible in the ECU environment in diesel vehicle.

$$\text{Residual NOx} = x_{NOx,\,fault} - x_{NOx,\,normal} \quad (30)$$

$$\text{Residual } NH_3 = x_{NH_3,\,fault} - x_{NH_3,\,normal} \quad (31)$$

$$\text{Residual temperature} = T_{fault} - T_{normal} \quad (32)$$

If the residual value is out of a specific range, it can be identified as a fault. Calibrating the thresholds is challenging because the sensor of a real vehicle is noisy. The thresholds have to be set properly false alarm due to noise and model error. If the thresholds are adjusted low, the fault becomes more detectable, but sensor noise can also be recognized as a fault. They are affected by sensitivity of the sensors in a real vehicle.

RESULTS AND DISCUSSION

In this study, two fault scenarios are considered: urea injector fault and ammonia storage capacity fault. A constant feed gas with 400 ppm NO and 100 ppm NO_2 flows into the catalyst system for 30 minutes. It is assumed that the initial ammonia adsorption sites are empty. The system fault is generated after the system reaches a steady state. The results of model-based fault detection are shown in Fig. 4. The simulations of urea-SCR system are run using MATLAB R2020a with Intel® Core™ i7-10700 CPU. It takes 291.6 seconds to simulate a 30-minute scenario.

Fig. 4(a) shows the residual values for urea solution injector fault, which causes decrease of urea injection. During the first 10 minutes, the SCR system reaches steady state where ammonia adsorption and desorption reactions are equilibrated. The fault is introduced in the urea-SCR system after 10 minutes of normal state simulation. The black dashed line indicates threshold level. After the fault is introduced, the NOx concentration gradually increases and exceeds the threshold within 13 minutes, but the ammonia concentration and temperature of outlet gas show just slight decreases without significant change. They could be detectable by adjusting the threshold level, but in such way, noise can be recognized as a system fault. If the urea solution injector does not work properly, it leads to decrease in the reducing agent, ammonia. As the amount of ammo-

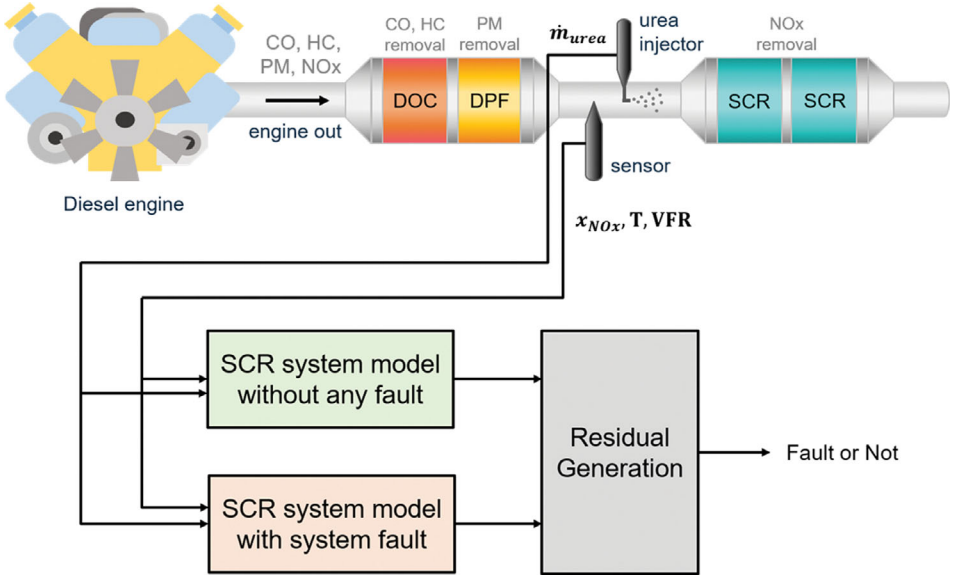

Fig. 3. Scheme of model-based fault detection for urea-SCR system.

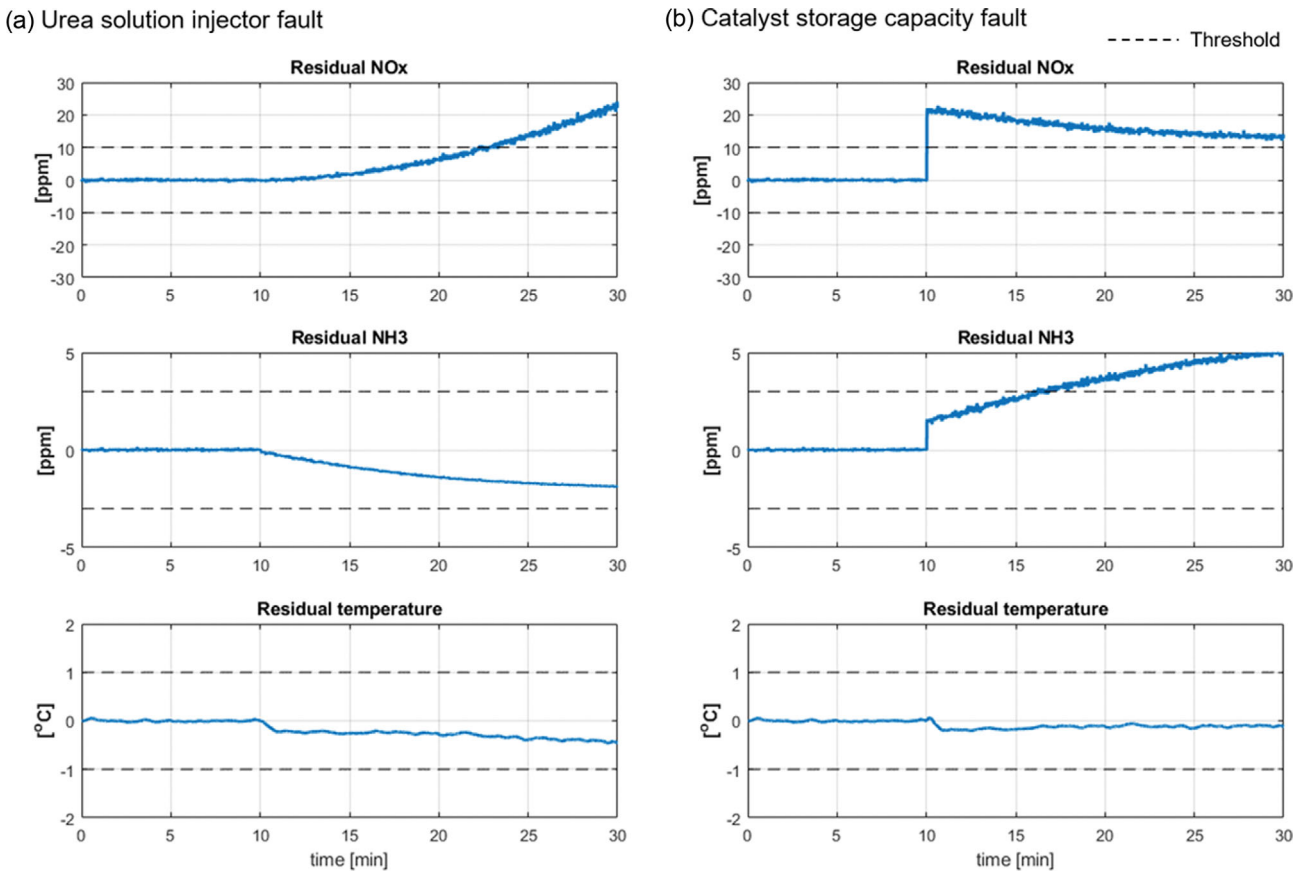

Fig. 4. Residuals for urea-SCR system (a) Urea solution injector fault (b) Catalyst storage capacity fault.

Table 1. Fault-symptom table for urea-SCR system (++: Symptom responds intense positive, +: symptom responds positive, o: symptom does not respond)

Fault	Residual NOx	Residual NH_3	Residual temperature
None	o	o	o
Urea injector	++	o	o
Catalyst deactivation	+	++	o

nia in the catalyst system is reduced, the SCR reaction of NOx is reduced, and thus the amount of NOx in outlet stream is increased. Ammonia has a small amount of emission even under normal conditions, so the residual is insignificant.

The results for model-based fault detection of ammonia storage capacity fault are shown in Fig. 4(b). This fault may occur due to hydrothermal aging and catalyst poisoning by sulfur. The ammonia storage capacity is decreased as the adsorption sites on the catalyst surface are reduced. This case often happens with old diesel vehicles. After ten minutes of normal state simulation, the fault is introduced by decreasing the ammonia storage capacity of both adsorption sites, S1 and S2. Both NOx concentration and ammonia concentration of outlet stream increase immediately after the occurrence of the system fault. The reduction reaction rate of nitrogen oxides is reduced as ammonia in the adsorbed stated is decreased.

The simplified symptoms for a single fault are shown in Table 1. It demonstrates that different symptoms appear for different system faults. The table can be used as a basis for fault diagnosis and fault-tolerant control of aftertreatment system.

CONCLUSIONS

This study presents a model-based fault detecting strategy for urea-SCR system of diesel vehicle. The proposed approach includes a first-principle modeling of urea-SCR system that considers SCR reactions, mass transfer and heat transfer. Through the successive linearization method, the one-dimensional model can be calculated in real time. Using the model, residuals are generated by simply comparing fault mode and fault-free mode. The suggested method effectively isolates two types of fault scenario: urea solution injector fault and catalyst's storage capacity fault. The results of this study are applicable to further fault-tolerant control of aftertreatment system, reducing NOx emissions of old diesel vehicles. However, there is a limitation in that it is difficult to calculate the model in real time at the current level of ECU performance. If ECU performance is improved, it is expected that it will be possible to diagnose the fault with

urea-SCR system and determine when to replace the equipment.

ACKNOWLEDGEMENT

This research was supported by the National Research Foundation of Korea (NRF) grant funded by the Korean Government (MSIT) [NRF-2016R1A5A1009592]. The Institute of Engineering Research at Seoul National University provided research facilities for this work.

NOMENCLATURE

Symbol

A_{wc-g} : surface area between washcoat and gas phase [m^2]
$C_{g,j}$: mole concentration of species *j* in gas phase [mol m^{-3}]
$C_{g,j}^{(n)}$: mole concentration of species *j* in gas phase at *n*th position [mol m^{-3}]
$C_{p,g}$: heat capacity of gas [J K^{-1}]
$C_{p,s}$: heat capacity of substrate [J K^{-1}]
$C_{p,wc}$: heat capacity of washcoat [J K^{-1}]
$C_{wc,j}$: mole concentration of species *j* in washcoat phase [mol m^{-3}]
d_h : hydraulic diameter of a channel [m]
$D_{mol,j}$: molecular diffusivity coefficient of species *j* in air [m2 s-1]
G_a : geometric surface area to catalyst volume ratio [m-1]
H_j^f : enthalpy of formation of species *j* [J mol^{-1}]
$k_{m,j}$: mass transfer coefficient of species *j* [m s^{-1}]
M_{air} : molecular mass of air [kg mol^{-1}]
M_j : molecular mass of species *j* [kg mol^{-1}]
$\dot{m}_{urea}$: mass flowrate of urea [kg s^{-1}]
p_0 : atmospheric pressure [Pa]
r_i : reaction rate of *i*th reaction [mol m^{-3} s^{-1}]
Sh : Sherwood number [-]
T_g : temperature of bulk gas [K]
$T_g^{(n)}$: temperature of bulk gas at *n*th position [K]
T_s : temperature of substrate [K]
T_{wc} : temperature of washcoat [K]
u_g : bulk gas velocity [m s^{-1}]
U_o : overall heat transfer coefficient [J m^{-2} K^{-1} s^{-1}]
V_g : volume of gas [m^3]
V_{wc} : volume of washcoat [m^3]
x_{NOx} : mole fraction of NOx [-]
ε_{wc} : washcoat porosity [-]
ε_1 : (volume of gas)/(volume of catalyst system) [-]
ε_2 : (volume of washcoat)/(volume of catalyst system) [-]
ε_3 : (volume of substrate)/(volume of catalyst system) [-]
θ_m : coverage fraction of *m*th site [-]
v_{ji} : reaction coefficient of species *j* in *i*th reaction [-]
ρ_g : density of gas [kg m^{-3}]
ρ_s : density of substrate [kg m^{-3}]
ρ_{wc} : density of washcoat [kg m^{-3}]
$\sigma_{j,air}$: collision diameter of species *j* [m]
ψ_m : storage capacity of *m*th site [mol m^{-3}]
$\Omega_{j,air}$: collision integral of species *j*

ABBREVIATIONS

DPF : diesel particulate filter
DOC : diesel oxidation catalyst
ECU : engine control unit
EGR : engine gas recirculation
HC : hydrocarbon
LNT : lean NOx trap
NOx : nitrogen oxides
OBD : on-board diagnostics
PM : particulate matter
RDE : real-driving emission
SCR : selective catalytic reduction
VFR : volumetric flowrate

REFERENCES

1. E. Furuholt, *Resour., Conserv. Recycl.*, **14**, 251 (1995).
2. H. L. MacLean and L. B. Lave, *Environ. Sci. Technol.*, **37**, 5445 (2003).
3. A. C. Lloyd and T. A. Cackette, *J. Air Waste Manage. Assoc.*, **51**, 809 (2001).
4. A. Russell and W. S. Epling, *Catal. Rev.*, **53**, 337 (2011).
5. S. Yang, C. Deng, Y. Gao and Y. He, *Adv. Mech. Eng.*, **8**, 1687814016637328 (2016).
6. K. Tsuneyoshi and K. Yamamoto, *Energy*, **48**, 492 (2012).
7. Z. Mera, N. Fonseca, J. N. López and J. Casanova, *Appl. Energy*, **242**, 1074 (2019).
8. T. Grigoratos, G. Fontaras, B. Giechaskiel and N. Zacharof, *Atmos. Environ.*, **201**, 348 (2019).
9. G. Busca, L. Lietti, G. Ramis and F. Berti, *Appl. Catal., B*, **18**, 1 (1998).
10. B. S. Kim, H. Jeong, J. Bae, P. S. Kim, C. H. Kim and H. Lee, *Appl. Catal., B*, **270**, 118871 (2020).
11. M. Shen, Z. Wang, X. Li, J. Wang, J. Wang, C. Wang and J. Wang, *Korean J. Chem. Eng.*, **36**, 1249 (2019).
12. D. W. Lee, S. J. Song and K. Y. Lee, *Korean J. Chem. Eng.*, **27**, 452 (2010).
13. J. H. Kwak, R. G. Tonkyn, D. H. Kim, J. Szanyi and C. H. Peden, *J. Catal.*, **275**, 187 (2010).
14. O. Kröcher, M. Devadas, M. Elsener, A. Wokaun, N. Söger, M. Pfeifer, Y. Demel and L. Mussmann, *Appl. Catal., B*, **66**, 208 (2006).
15. Y. Kim, T. Park, C. Jung, C. H. Kim, Y. W. Kim and J. M. Lee, *IEEE Trans. Control Syst. Technol.*, **27**, 2305 (2018).
16. S. D. Yim, S. J. Kim, J. H. Baik, I. S. Nam, Y. S. Mok, J. H. Lee, B. K. Cho and S. H. Oh, *Ind. Eng. Chem. Res.*, **43**, 4856 (2004).
17. H. Sjövall, R. J. Blint, A. Gopinath and L. Olsson, *Ind. Eng. Chem. Res.*, **49**, 39 (2010).
18. M. Koebel, G. Madia and M. Elsener, *Catal. Today*, **73**, 239 (2002).
19. M. Devadas, O. Kröcher, M. Elsener, A. Wokaun, N. Söger, M. Pfeifer, Y. Demel and L. Mussmann, *Appl. Catal., B*, **67**, 187 (2006).
20. H. JeffevS and A. Douglas, *SAE*, 942057 (1994).
21. Y. Y. Wang, Y. Sun, C. F. Chang and Y. Hu, *IEEE Trans. Veh. Technol.*, **65**, 4645 (2015).
22. K. Wijayanti, S. Andonova, A. Kumar, J. Li, K. Kamasamudram, N. W. Currier, A. Yezerets and L. Olsson, *Appl. Catal., B*, **166**, 568 (2015).
23. J. H. Kwak, D. Tran, S. D. Burton, J. Szanyi, J. H. Lee and C. H. Peden, *J. Catal.*, **287**, 203 (2012).
24. D. Depcik, D. Assanis and K. Bevan, *Int. J. Engine Res.*, **9**, 57 (2008).
25. R. B. Bird, *Appl. Mech. Rev.*, **55**, R1 (2002).

26. M. Bhattacharya, M. P. Harold and V. Balakotaiah, *AIChE J.*, **50**, 2939 (2004).
27. J. Welty, G. L. Rorrer and D. G. Foster, John Wiley & Sons (2020).
28. S. Lim, B. Lee, S. Choi, Y. Kim and J. M. Lee, *Ind. Eng. Chem. Res.*, **61**, 13523 (2022).
29. J. H. Lee and N. L. Ricker, *Ind. Eng. Chem. Res.*, **33**, 1530 (1994).
30. M. F. Hsieh and J. Wang, *IEEE Trans. Control Syst. Technol.*, 19.6 (2011).
31. H. Lee, C. Kim, D. H. Jeong and J. M. Lee, *Korean J. Chem. Eng.*, **38**, 2406 (2021).
32. M. Madakyaru, F. Harrou and Y. Sun, *Process Saf. Environ. Prot.*, **107**, 22 (2017).
33. S. Simani, C. Fantuzzi and R. J. Patton, Springer, London, 19 (2003).
34. F. Kimmich, A. Schwarte and R. Isermann, *Control Eng. Pract.*, **13**, 189 (2005).
35. R. Isermann, *Annu. Rev. Control*, **29**.1 (2005).
36. J. Gertler, *Control Eng. Pract.*, **5**.5 (1997).